Limits of mechanical energy storage and structural changes in twisted carbon nanotube ropes

Zacharias G. Fthenakis,[1] Zhen Zhu,[1] David Teich,[2] Gotthard Seifert,[2] and David Tománek[1,*]
[1]*Physics and Astronomy Department, Michigan State University, East Lansing, Michigan 48824, USA*
[2]*Physikalische Chemie, Technische Universität Dresden, D-01062 Dresden, Germany*
(Received 22 July 2013; published 2 December 2013)

Arrays of twisted carbon nanotubes and nanotube ropes are equivalent to a torsional spring capable of storing energy. The advantage of carbon nanotubes over a twisted rubber band, which is used to store energy in popular toys, is their unprecedented toughness. Using *ab initio* and parametrized density functional calculations, we determine the elastic range and energy storage capacity of twisted carbon nanotubes and nanotube ropes. We find that a twisted nanotube rope may reversibly store energy by twisting, stretching, bending, and compressing constituent nanotubes. We find that in the elastic regime, the interior of a twisted rope encounters hydrostatic pressures of up to tens of GPa. We examine the limits of reversible energy storage and identify structural deformations beyond the elastic limit, where irreversibility is associated with breaking and forming new covalent bonds. Under optimum conditions, the calculated reversible mechanical energy storage capacity of twisted carbon nanotube ropes surpasses that of advanced Li-ion batteries by up to a factor of 4 to 10.

DOI: 10.1103/PhysRevB.88.245402 PACS number(s): 61.48.De, 62.25.−g, 61.46.−w

I. INTRODUCTION

Reversible energy storage is a topic of global importance that calls urgently for improved storage media.[1,2] Common energy storage mechanisms include gravitational potential energy in water reservoirs, electrical potential energy in capacitors and batteries, nuclear potential energy in unstable isotopes, chemical potential energy in fossil fuels and explosives, and thermal energy in steam. Mechanical energy storage, used in wind-up watches and flywheels, has so far received less attention for large-scale applications. The figure of merit for energy storage media includes volumetric and gravimetric energy density (i.e., stored energy per unit volume or per unit mass of the storing medium), power delivery, practical recovery efficiency, ease of use, and portability. With an energy density of 0.72 MJ/kg, Li-ion batteries have evolved into one of the most popular cyclable energy carriers.[2] Advances in nanomaterials, in particular carbon nanotubes (CNTs) with an unprecedented toughness,[3] invite us to revisit nanomechanical energy storage. The incentive for such a study is an unusually high deformation energy density predicted for reversibly twisted carbon nanotube ropes[4] as well as experimental progress in using carbon nanotubes as artificial muscles[5–7] and high-performance springs.[8,9]

Our study explores the usefulness of twisted carbon nanotubes and carbon nanotube ropes as nanomechanical energy carriers. To address this aspect of carbon nanotubes, we performed atomistic *ab initio* and parametrized calculations for a torsional spring consisting of a carbon nanotube bundle. The advantage of carbon nanotubes over a twisted rubber band that stores energy in popular toys is their elastic behavior and resilience that leads to an unprecedented energy storage capacity. Our results not only establish the elastic limits of a stretched, twisted, bent, and compressed carbon nanotube rope, but also identify the microscopic decay processes in the inelastic regime. We find that within the elastic regime, internal pressure inside a twisted carbon nanotube rope may rise up to tens of GPa. Mapping our results onto continuum elasticity theory allows us to decompose the energy in a twisted rope into stretching, twisting, bending, and compression contributions. Our results indicate that reversible mechanical energy storage capacity of carbon nanotube systems surpasses that of advanced Li-ion batteries by up to one order of magnitude in the ideal case.

Past theoretical studies have mostly investigated deformations associated with torsion, stretching, and bending of individual nanotubes.[10–15] Whereas all these modes occur also in a nanotube rope, their intimate inter-connection during the torsion of a rope has not been addressed adequately in previous studies. As we discuss in the following, twisting a rope subjects especially nanotubes at its surface to stretching. The stretched nanotubes in turn subject the interior of the rope to high hydrostatic pressures. This is the microscopic counterpart to the well-known fact that excess water in a wet cloth can be eliminated more efficiently by wringing than by squeezing. We investigate this aspect of nanotube rope torsion, which has been neglected so far, in more detail and identify possible structural changes in closely packed, hydrostatically compressed nanotube arrays.

II. METHODS

Deformation energy of isolated and bundled carbon nanotubes is calculated using *ab initio* density functional theory (DFT), as implemented in the SIESTA code.[16] We utilize the Ceperley-Alder exchange-correlation formalism[17] as parametrized by Perdew and Zunger[18] and norm-conserving Troullier-Martins pseudopotentials[19] in the Kleinman-Bylander factorized form.[20] The systems of interest are described using a double-zeta basis, including polarization orbitals, and periodic boundary conditions for all calculations. We sample the Brillouin zone of the periodic nanotube array by a $2 \times 2 \times 8$ k-point grid. The spatial extent of the localized orbitals is limited in such a way[21] that the energy shift caused by their spatial confinement does not exceed 10 meV. The charge density and potentials are determined on a real-space grid with a mesh cutoff energy of 100 Ry, which is sufficient to achieve a total energy convergence of better than 0.1 meV/unit cell during the self-consistency iterations. All geometries are

optimized using the conjugate gradient method,[22] until none of the residual Hellmann-Feynman forces exceed 0.04 eV/Å. For calculations of nanotube arrays under hydrostatic pressure, the tolerance of the stress tensor was set to 0.1 GPa.

Since description of twisted nanotubes using conventional periodic boundary conditions requires very large unit cells in the axial direction, we use the density functional based tight-binding (DFTB) (Ref. 23) adaptation of a simplified density functional theory with a local orbital basis to systems with helical symmetry[24–26] to study deformations caused by torsion. The helical unit cells used in a helical nanotube are a counterpart of axial unit cells in a straight nanotube. This total energy functional had been applied successfully to a variety of carbon structures[23] and subsequently extended to accommodate van der Waals interactions,[27] including their proper description in graphitic systems.[27] Use of helical symmetry, which allowed proper description of chiral nanotubes in the past,[15,26,28] turned out also to be essential to efficiently describe the geometry and energy changes in twisted nanotubes and nanotube ropes.

As a counterpart to atomistic simulations, we provide simple analytical estimates of the deformation energy and the associated energy storage potential under optimum conditions. The main benefit of such estimates is their universality and physical transparency.

III. RESULTS AND DISCUSSION

In the following, we determine the behavior of nanotubes and nanotube ropes subject to different kinds of external stress. We first discuss results of atomistic simulations that reveal structural and energetic changes as individual nanotubes are twisted, stretched, bent, and radially compressed in a rope. We consider the most abundant (10,10) armchair nanotubes and their (18,0) zigzag counterparts with the similar diameter of 1.4 nm, as well as narrower and wider nanotubes. These data reveal the elastic limits and provide the foundation for a continuum elasticity description within the elastic regime. This approach is very useful for large systems with many nanotubes, which can not be treated with atomistic simulations. The continuum elasticity approach not only provides a way to estimate energy storage in ropes with many nanotubes, but also elucidates the interplay between the different deformation modes and provides a guideline to maximize energy storage in a particular nanotube system.

A. Twisting of nanotubes

To characterize the deformation of a nanotube twisted about its own axis, we first associate the angle φ with the axial rotation of the nanotube cross section along a tube segment of length l_0 and define the twist rate by φ/l_0. Using radian units for φ, we may further define the dimensionless twist strain by

$$\epsilon_\circ = d_{(n,m)}\varphi/l_0, \tag{1}$$

where $d_{(n,m)}$ is the diameter of an (n,m) nanotube, approximately given by $d_{(n,m)} = 0.783(n^2+m^2+nm)^{1/2}$ Å. Here, we wish to point out that the present definition of $\epsilon_\circ$ differs from that used in Ref. 4.

The torsion energy per atom $\Delta E_t/N$ in (10,10) and (5,5) carbon nanotubes is presented in Fig. 1(a). To reduce the effect of constraints imposed by the helical symmetry, our helical unit cell was composed of four primitive unit cells, corresponding to 160 atoms for the (10,10) nanotube and 80 atoms for the (5,5) nanotube. Our results in Fig. 1(a) indicate that initially undeformed nanotubes keep their circular cross section when twisted up to a critical rate $\epsilon_{\circ,\mathrm{crit}} \gtrsim 0.5$ rad. Exceeding $\epsilon_{\circ,\mathrm{crit}}$ induces spontaneous flattening in the nanotube, which is maintained even when the twist rate is gradually reduced, giving rise to hysteretic behavior. Consequently, the energetically more favorable flattened geometry, shown in the structural snap shots in Fig. 1(b), is locally stable even at twist rates $\epsilon_\circ < \epsilon_{\circ,\mathrm{crit}}$. Structural deformations of a (10,10) nanotube subject to twisting are shown as a movie in the Supplemental Material.[29]

We find that the critical twist strain, at which the circular cross section becomes unstable, is $\epsilon_{\circ,\mathrm{crit}}(10,10) = 0.52$ rad for the (10,10) and at a very similar value $\epsilon_{\circ,\mathrm{crit}}(5,5) = 0.57$ rad for the (5,5) nanotube. We use the lower of these values, $\epsilon_\circ = 0.52$ rad, as a realistic estimate of the elastic limit, which we present in Table I. We conclude that the deformation energy associated with twisting may reach up to ≈1 eV/atom, a significant fraction of the 7.3 eV/atom binding energy in graphitic carbon, in the reversible elastic regime $\epsilon_\circ < \epsilon_{\circ,\mathrm{crit}}$. As seen in Fig. 1(a), the deformation energy drops to ≈0.4 eV/atom due to flattening at $\epsilon_{\circ,\mathrm{crit}}$ and slowly increases within increasing twist rate. This consideration will be important when discussing realistic energy storage in twisted nanotube ropes later on.

Within the elastic regime, a nanotube subject to torsion can be viewed as a torsional spring with torsional energy per atom given by

$$\Delta E_t/N = k_\circ \epsilon_\circ^2 . \tag{2}$$

Quadratic fits to the calculated values of the torsional energy $\Delta E_t/N$ in not flattened nanotubes, shown by the solid line for the (10,10) and the dashed line for the (5,5) nanotube in Fig. 1(a), yield $k_\circ(10,10) = 3.14$ eV/rad^2 for the (10,10) and $k_\circ(5,5) = 2.94$ eV/rad^2 for the (5,5) nanotubes. Since these values are very similar, we list $k_\circ(10,10)$ as a representative value in Table I. This behavior is indeed expected since twisting a nanotube corresponds locally to shearing a graphene monolayer. As suggested above, the optimum energy storage in the hysteretic regime, where twisted nanotubes are flattened, is reduced by up to 60%.

B. Stretching of nanotubes

Unlike twisting, stretching does not change the number of atoms in the axial unit cell and can thus be studied by both DFT and DFTB. We characterize the degree of axial stretching of a nanotube by the axial strain

$$\epsilon_\parallel = (l - l_0)/l_0, \tag{3}$$

where l is the length of the stretched and l_0 that of the initial unstretched nanotube segment.

Our results for the stretching energy per atom $\Delta E_s/N$ as a function of $\epsilon_\parallel$ are presented in Fig. 1(c) for (10,10) and (18,0) carbon nanotubes. The DFTB calculations have been

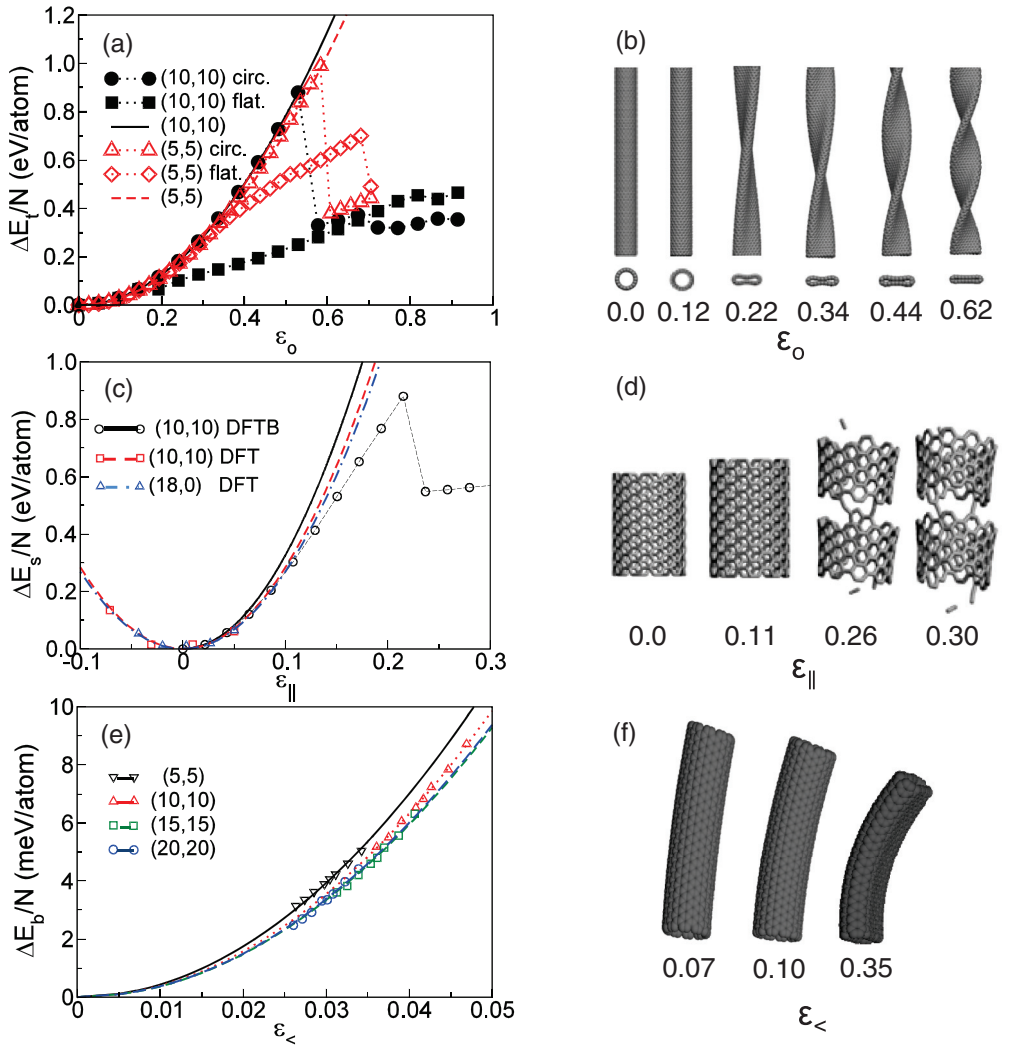

FIG. 1. (Color online) Energy investment and structural snap shots of an isolated carbon nanotube subject to torsion [(a), (b)], stretching [(c, (d)], and bending [(e), (f)]. (a) Twist energy per atom $\Delta E_t/N$ as a function of the dimensionless twist strain $\epsilon_\circ$ of (10,10) and (5,5) nanotubes with metastable circular or flattened cross sections. (c) Stretch energy per atom $\Delta E_s/N$ of isolated and bundled (10,10) and (18,0) nanotubes as a function of the axial strain $\epsilon_\parallel$. (e) Bending energy per atom $\Delta E_b/N$ as a function of the bending strain $\epsilon_\angle$ for individual (5,5), (10,10), (15,15), and (20,20) nanotubes. Structural snap shots in (b), (d), and (f) are presented for the (10,10) nanotube. Only the low-energy branch of flattened nanotubes is presented in (b). All results, except where specified otherwise, are based on DFTB.

TABLE I. Energy storage in deformed carbon nanotubes and periodic nanotube arrays. $\Delta E/N$ represents the maximum deformation energy per atom for a particular deformation mode and J gives the corresponding gravimetric energy density.

Deformation mode	Force constant (eV)	Elastic limit	$\Delta E/N$ (eV)	J (MJ/kg)
Twisting[a]	$k_\circ = 3.14$	$\epsilon_\circ = 0.52$	0.849	6.82
Stretching	$k_\parallel = 32.5$	$\epsilon_\parallel = 0.12$	0.468	3.76
Bending[a]	$k_\angle = 3.94$	$\epsilon_\angle = 0.21$	0.172	1.38
Compression (A)[b]	$k_\perp = 5.32$	$\epsilon_\perp = 0.19$	0.576	4.62
Compression (A)[c]	$k_\perp = 5.89$	$\epsilon_\perp = 0.15$	0.381	3.91
Compression (C)[b,c]	$k_\perp = 1.50$	$\epsilon_\perp = 0.19$	0.162	1.29

[a]Deformation maintaining circular cross section.
[b]Deformation maintaining triangular lattice symmetry.
[c]Deformation under hydrostatic pressure.

performed for an isolated nanotube and the DFT calculations for a triangular lattice of nanotubes in equilibrium separation. Our DFT calculations utilize the primitive unit cells containing 40 atoms in the (10,10) and 72 atoms in the (18,0) nanotube. To reduce artifacts of constraints associated with finite unit cells, our axial unit cell in DFTB was composed of four primitive unit cells, corresponding to 160 atoms for the (10,10) nanotube. The benefit of large supercells becomes obvious at the point of fracture that is induced by dislocations[11] and depicted in Fig. 1(d). Structural deformations of a (10,10) nanotube subject to stretching are shown as a movie in the Supplemental Material.[29] Our calculated critical strain value $\epsilon_{\parallel,\mathrm{crit}} \approx 22\%$, associated with the point of fracture, likely overestimates the behavior of nanotubes containing defects at nonzero temperature. Therefore, we list the lower observed value[30] $\epsilon_{\parallel,\mathrm{crit}}^{\mathrm{expt.}} \approx 12\%$ as the limit of the elastic regime in Table I. Similar to torsion, we find that the deformation energy

associated with stretching a nanotube in the reversible regime may reach up to ≈0.5 eV/atom, a significant fraction of the cohesive energy.

Within the elastic regime, a stretched nanotube can be viewed as a linear spring, with stretching energy per atom given by

$$\Delta E_s/N = k_\parallel \epsilon_\parallel^2. \quad (4)$$

Quadratic fits to the calculated values of the stretching energy $\Delta E_s/N$ are shown by solid and dashed lines for the different nanotubes in Fig. 1(c). The DFT data are best reproduced by $k_\parallel(10,10) = 28.4$ eV for the (10,10) and $k_\parallel(18,0) = 26.9$ eV for the (18,0) nanotubes. The similarity of the values obtained for the two nanotubes with a similar diameter reflects the fact that the elastic behavior of nanotubes is primarily determined by the diameter and only to a much lesser degree by the chiral index. The DFTB data for the (10,10) nanotube are best reproduced by $k_\parallel(10,10) = 32.5$ eV. In view of the different constraints used in DFT and DFTB calculations, the calculated values are in reasonable agreement. For the sake of consistency, we list the DFTB value for the (10,10) nanotube in Table I.

C. Bending of nanotubes

In a twisted nanotube rope, individual nanotubes are also deformed by bending. To characterize bending, we define the bending strain as

$$\epsilon_\angle = d_{(n,m)}/R, \quad (5)$$

where $d_{(n,m)}$ is the nanotube diameter and R the local radius of the bending curvature. Our results for the bending energy per atom $\Delta E_b/N$ as a function of $\epsilon_\angle$ are presented in Fig. 1(e) for (5,5), (10,10), (15,15), and (20,20) nanotubes. The numerical results are based on total energy calculations for an infinite nanotube helix using the DFTB code. The bending energy was determined by subtracting torsion and stretching deformation components from total energy differences. These results were found to agree with discrete results for finite nanotube tori that could also be treated using specific helical boundary conditions.

Considering a nanotube to be represented by an elastic beam, the bending energy per atom should be described by

$$\Delta E_b/N = k_\angle \epsilon_\angle^2. \quad (6)$$

We find indeed that our data in Fig. 1(e) are well described by this expression. The optimum continuum elasticity representation of the numerical data, presented by lines in Fig. 1(e), uses $k_\angle(5,5) = 4.38$ eV for the (5,5) nanotube, $k_\angle(10,10) = 3.94$ eV for the (10,10) nanotube, $k_\angle(15,15) = 3.71$ eV for the (15,15) nanotube, and $k_\angle(20,20) = 3.75$ eV for the (20,20) nanotube. Since these values are very similar, for the sake of consistency, we represent them by the value obtained for the (10,10) nanotube in Table I. Inspection of the bending energy values in Fig. 1(e) indicates that the energetic contribution of this deformation is significantly smaller than that of twisting and stretching, in particular for relatively low bending strains found in twisted nanotube ropes. Nanotube deformations in this regime are depicted in Fig. 1(f). We associate the limit of the elastic regime with the onset of buckling or kinking[4] near $\epsilon_\angle = 0.21$ and list this value in Table I. As we will show in the following, effective values of $\epsilon_\angle$ in nanotube ropes twisted to the elastic limit are rather small, so that buckling or kinking should be of no concern.

D. Compression of nanotube arrays

As mentioned above, twisting a nanotube rope subjects its interior to hydrostatic pressure. To explore this aspect of energy storage in carbon nanotube ropes, we performed DFT calculations for a close-packed lattice of (18,0) nanotubes subject to hydrostatic pressure. Our results, presented in Fig. 2, depict changes in the total energy and equilibrium structure of the system.

Following indications that the interior of a twisted nanotube rope may be subject to tens of GPa pressure and that significant structural changes occur in an ideal triangular nanotube lattice under uniform compression,[4] we have studied in more detail how nanotube arrays behave under hydrostatic pressure. The equilibrium arrangement of (18,0) carbon nanotubes at zero pressure is a triangular lattice, depicted in cross section near the top of Fig. 2(a). With no constraints on the shape of the unit cell, we found that nanotubes subject to moderate pressures $p \approx 1$ GPa may deform at least in four different ways, which we label A, B, C, and D. Structural deformations of (18,0) nanotube arrays compressed along these pathways are shown as movies in the Supplemental Material.[29]

As seen in Fig. 2(a), the individual nanotubes maintain the sixfold symmetry of the lattice along the deformation pathways A and B up to $p \approx 30$ GPa, with the nanotube cross sections deforming to a hexagon or a star. The underlying lattice remains triangular, albeit with a decreasing lattice constant. Deformation pathways C and D, on the other hand, involve nanotubes undergoing elliptical deformation of their cross section and a significant distortion of the initial triangular lattice. The relative stability of the individual structures, shown as compression energy per atom $\Delta E_c/N$ in Fig. 2(b), suggests that symmetry breaking along pathways C and D is energetically favorable. The increase in mass density ρ_g with increasing hydrostatic pressure, shown in Fig. 2(c), is particularly dramatic near $p \approx 3$ GPa for pathway C and $p \approx 5$ GPa for pathway D, where nanotubes become flattened, turning into bilayer graphene nanoribbons that start connecting to graphene layers. Conversion to graphite, depicted in Fig. 2(a), completes at pressures $\gtrsim$8 GPa.

Under pressures exceeding $p \approx 30$ GPa, pathways A and B describe a plastic deformation to a rigidly connected foamlike structure[31] with an increasing fraction of sp^3 bonded carbon atoms, as seen in Fig. 2(d). We observe a rapid energy rise along pathways A and B in the elastic regime, reaching $\Delta E_c \approx 0.8$ eV/atom at $p \approx 30$ GPa, close to the energy storage limits associated with reversible torsion and stretching of individual nanotubes. Pathways C and D display a lower-energy storage potential $\Delta E_c \approx 0.1$ eV/atom before flattened nanotubes convert to nanoribbons and graphite.

When describing compression energy in a rope with a finite number N_s of nanotube strands, we will need to distinguish nanotubes at the surface with fewer neighbors from nanotubes in the interior of the rope. Then, it is useful to decompose our results for the compression energy ΔE_c of an infinite nanotube

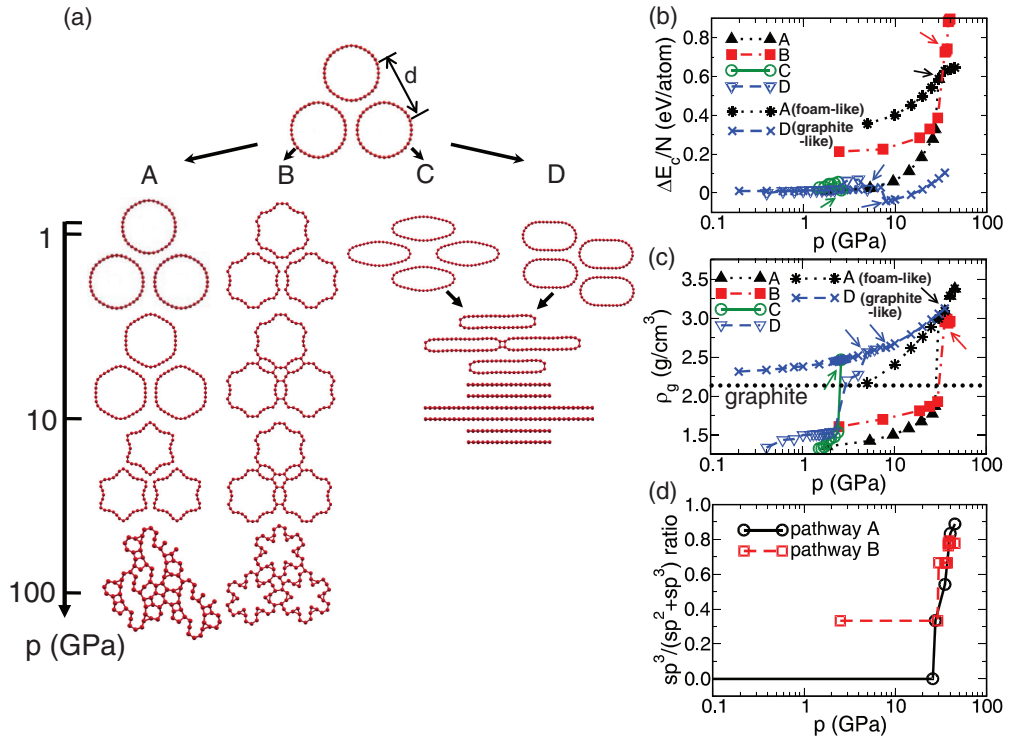

FIG. 2. (Color online) Changes in the total energy and equilibrium structure of a close-packed lattice of (18,0) nanotubes subject to hydrostatic pressure. (a) Structural changes during deformation pathways A, B, C, and D as a function of pressure, defined by the scale on the left, in end-on view. (b) Compression energy per atom $\Delta E_c/N$, (c) mass density ρ_g, and (d) fraction of sp^3 bonded carbon atoms as a function of hydrostatic pressure p. Conditions for abrupt structural changes are indicated by arrows.

array into pairwise interactions $\Delta E_{c,ij}$ between neighboring tubes i and j. For small deformations in the elastic regime, the compression energy per atom $\Delta E_c/N$ can then be expressed as

$$\Delta E_c/N = \sum_{i>j} \Delta E_{c,ij}/N, \quad \text{where}$$
$$\Delta E_{c,ij}/N = k_\perp \epsilon_{\perp,ij}^2/N_s. \tag{7}$$

Here, the summation extends over nearest-neighbor nanotubes only and $k_\perp$ is the compression force constant. The compression strain of a pair of nanotubes separated by the intertube distance d_{ij} is given by

$$\epsilon_\perp(i,j) = (d_0 - d_{ij})/d_0. \tag{8}$$

Here, d_{ij} represents the actual and d_0 the equilibrium intertube distance, defined as interaxial distance, at zero pressure. For a pair of nanotubes in a compressed lattice, $k_\perp$ depends on the specific tube deformation and relative tube orientation and is thus not as well defined as $k_\parallel$, $k_\circ$, and $k_\angle$. We present $k_\perp$ values along with the limiting elastic deformation values in Table I for the different pathways.

A relatively straightforward way to identify experimentally the onset of both types of plastic deformations is to trace changes in the radial breathing mode (RBM). We obtained the vibration spectrum of nanotube arrays under pressure using a Fourier transform of the velocity-velocity autocorrelation function in DFT molecular dynamics simulations. Our results indicate a blue-shift of the RBM with increasing pressure along pathway C. We expect this blue-shift to occur also along different pathways, and the RBM to disappear at the onset of plastic deformation.

It is worth noting that structural changes induced in the plastic regime under high pressures are permanent. In other words, the foamlike structures formed at $p > 30$ GPa along pathways A and B as well as graphene nanoribbons and graphite formed along pathways C and D remain stable and do not convert back to a nanotube array under decompression down to $p = 0$. Even though we have not observed such structures in atomistic simulations of twisted nanotube ropes, we need to point out that also these foam and graphitic phases deform under high pressures and thus may be used to store energy, as indicated by the corresponding data in Fig. 2(b).

As part of our investigation, we also studied the effect of compression-induced structural changes on the response of nanotubes to tensile stress along the different pathways. To obtain this information, we calculated the stretching energy ΔE_s using DFT for different values of intertube distances d as a function of the axial strain $\epsilon_\parallel$. We found that our results can be well reproduced using Eq. (4) in the elastic regime and present the fitted force constants $k_\parallel$ for a lattice of (18,0) as well as (10,10) nanotubes in Table II.

Results in Table II suggest that intertube interactions and radial compression do not cause significant changes in the axial stretching constant $k_\parallel$. This is a strong indication that stretching and compression are nearly decoupled. Small differences between different pathways may be linked to the occurrence of sp^3 hybridization along pathway B and its absence along pathways A and C.

TABLE II. Force constants $k_{\|}$ for axial stretching of (18,0) and (10,10) nanotubes in a close-packed lattice with intertube separation d.

System	d (Å)	$k_{\|}$ (eV)
(18,0) lattice (pathway A)	14.6–17.0	26.0–27.8
(18,0) lattice (pathway B)	14.6–15.0	24.0–24.6
(18,0) lattice (pathway C)	14.6	26.0
(10,10) lattice	15.8–17.0	28.4–29.2

E. Equilibrium geometry of a twisted nanotube rope

A finite bundle or rope of nanotubes is represented in the schematic Fig. 3(a). Each nanotube strand of diameter $d_{(n,m)}$ in the rope is characterized by a coil of radius ρ and pitch length λ. The coil geometry is the result of twisting, stretching, bending, and radially compressing an initially straight free-standing nanotube segment. So far, we have studied twisting, stretching, and bending of each individual nanotube strand as well as compression of nanotube arrays as decoupled deformation mechanisms. In a twisted nanotube rope, these deformations occur simultaneously and are coupled.

The coupling of deformation modes can be understood as follows. Considering nanotubes in the outermost layer of the rope, it is intuitively clear that twisting a rope causes these nanotubes not only to twist and bend, but also to stretch at an energy cost. To reduce the stretching energy, the surface nanotube layer compresses the interior of the rope at the expense of the compression energy in order to reduce the axial stretching energy. When a rope with a finite number of nanotube strands is subject to a given twist strain $\epsilon_\circ$, each nanotube strand undergoes twisting, stretching, bending, and compression in a particular optimum way that minimizes the total energy. The optimum geometry of selected nanotube ropes is shown in Fig. 3(b) in end-on view and in Fig. 3(c) in side view. Movies depicting structural changes in twisted nanotube ropes are presented in the Supplemental Material.[29]

To determine the equilibrium geometry of a twisted rope, we study in the following the contribution of all concerted deformations to the total energy.

F. Total energy of a twisted nanotube rope

To determine the twist rate that limits the elastic regime and to estimate the upper limit of energy storage in a twisted nanotube rope, we combine in the following our results for individual deformation modes. The total energy per atom $\Delta E/N$, which is stored in a twisted nanotube rope, contains contributions from twisting, stretching, and bending of each

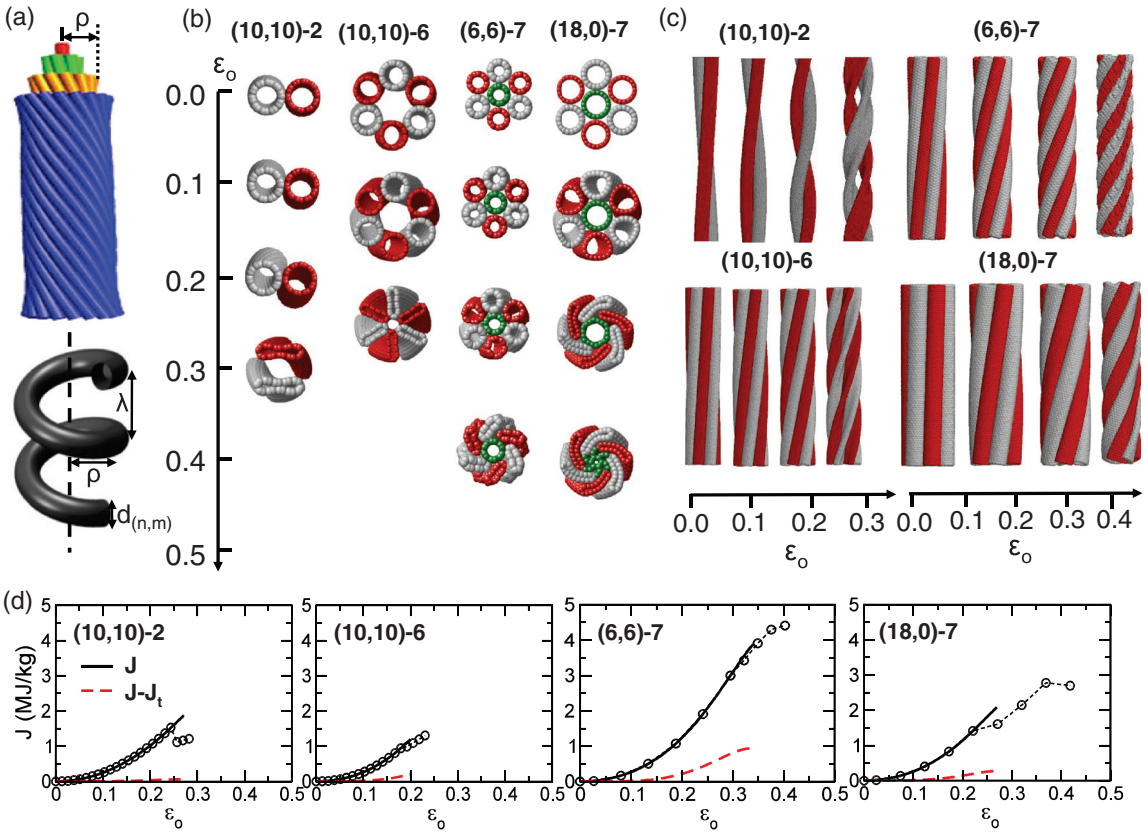

FIG. 3. (Color online) Structural deformations and energy storage in twisted nanotube ropes. (a) Schematic of a rope, where individual nanotube strands of diameter $d_{(n,m)}$ form coils defined by radius ρ and pitch length λ. (b) End-on and (c) side view of twisted ropes with different numbers of (n,m) nanotube strands at different values of the twist strain $\epsilon_\circ$. (d) Total gravimetric energy storage density J of these ropes. DFTB results are represented by the data points. The solid lines are fits to these data points using Eq. (11). The red dashed lines represent the contribution of all energy storage mechanisms except twisting, based on Eq. (12). The notation $(n,m) - N_s$ describes a rope containing N_s strands of (n,m) nanotubes.

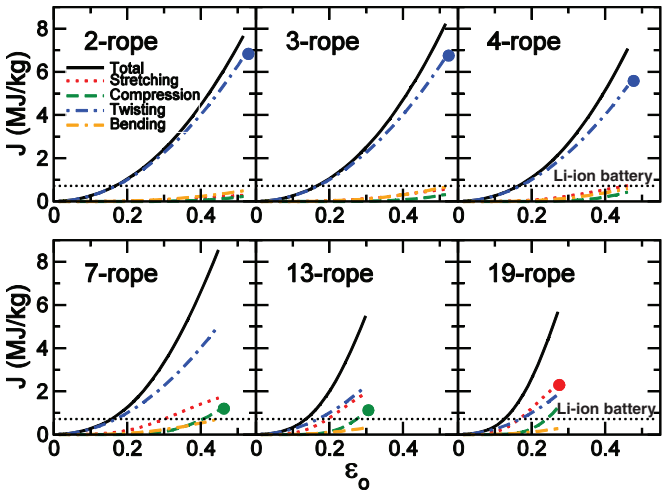

FIG. 4. (Color online) Gravimetric energy storage density J and its components as a function of the dimensionless twist strain $\epsilon_\circ$ in ropes containing 2–19 (10,10) nanotubes. Solid dots indicate branches of those mechanisms, where the elastic limit has been reached first. The dotted line indicates the maximum energy storage density of a Li-ion battery.

of the N_s nanotube strands, as well as the rope compression energy. In the elastic regime, it is given by

$$\Delta E/N = \Delta E_t/N + \Delta E_s/N + \Delta E_b/N + \Delta E_c/N \quad (9)$$

$$= k_\circ \epsilon_\circ^2 + k_\parallel \frac{1}{N_s}\sum_{i=1}^{N_s} \epsilon_{\parallel,i}^2 + k_\angle \frac{1}{N_s}\sum_{i=1}^{N_s} \epsilon_{\angle,i}^2 + k_\perp \frac{1}{N_s}\sum_{i>j} \epsilon_{\perp,ij}^2. \quad (10)$$

The summations extend over all N_s nanotube strands except in the last term, where the summation covers only pairs of adjacent nanotubes. In this expression, $\Delta E/N$ depends on $\epsilon_\circ$, which is the same for the rope and each nanotube strand, as well as $\epsilon_{\parallel,i}, \epsilon_{\angle,i}$ for each nanotube i and $\epsilon_{\perp,ij}$ for each nanotube pair. Using this expression, the energy storage in twisted ropes can be calculated by first minimizing $\Delta E/N$ with respect to these strains, taking into account the interrelation between them, as given by Eqs. (A1) and (A2) in the Appendix. The energy per atom can then be converted to the total gravimetric energy density J using $J = (\Delta E/N)/(12 m_p)$, where m_p is the atomic mass unit, $m_p = 1.67 \times 10^{-27}$ kg. Gravimetric energy storage density and its components, which have been determined in this way using Eq. (10), are shown in Fig. 4 for ropes containing 2–19 strands of (10,10) nanotubes.

Our results in Fig. 4 indicate that twisting dominates energy storage in ropes with 2–4 nanotube strands. With increasing number of nanotube strands, as the overall rope diameter increases, the role of stretching gains in importance. As indicated earlier, the resilience of nanotubes to being stretched is the main reason for compression in the interior of the rope. In ropes with 7–13 nanotubes, we find that the compressive strain reaches the elastic limit first. In wide ropes containing more than 19 nanotubes, the elastic regime is limited by stretching of nanotubes in the outermost layer. Even though the significance of bending nearly reached that of compression in the 7-rope, we have never found a case in our studies where the elastic range was limited by bending.

Each of the deformation mechanisms has its own elastic limit and a maximum gravimetric energy storage density, listed in Table I. Since the deformation mechanisms in a rope are coupled, the energy storage is limited by the mechanism, where the elastic limit is reached first. As we will show in the following, depending on the number and type of nanotubes in the rope, we find that reversible energy storage may be limited by twisting, compression, or stretching. Deformation mechanisms that limit the elastic regime of a particular rope are terminated by solid dots in Fig. 4.

For a given geometry, characterized by values $\epsilon_\circ$, $\epsilon_{\parallel,i}$, $\epsilon_{\angle,i}$, and $\epsilon_{\perp,ij}$ for all nanotubes and nanotube pairs, Eq. (10) provides a useful way to determine the deformation energy $\Delta E/N$ of a rope. Unfortunately, this expression says little about the indirect dependence of $\epsilon_{\parallel,i}$, $\epsilon_{\angle,i}$, and $\epsilon_{\perp,ij}$ on the twist strain $\epsilon_\circ$ of the entire rope. To help understand the relative significance of the individual energy contributions, we derive in the Appendix analytical expressions for the dependence of axial stretching, bending, and compression strains on the dimensionless twist strain $\epsilon_\circ$ of the rope. As we show in the Appendix, the energy density at low strain rates is given by

$$\Delta E/N = \Delta E_t/N + \Delta E_r/N, \quad (11)$$

where the torsional energy per atom $\Delta E_t/N$ is given by Eq. (2), and the remaining energy terms are given by

$$\Delta E_r/N \approx k_1 \epsilon_\circ^4 + k_2 \epsilon_\circ^8 + O(\epsilon_\circ^{12}). \quad (12)$$

We wish to point out that Eq. (11) is equivalent to Eq. (A10) in the Appendix. The gravimetric energy density estimated using Eq. (11) is shown in Fig. 3(d), with J corresponding to $\Delta E/N$ and $J - J_t$ to $\Delta E_r/N$. The coefficients $k_\circ$, k_1, and k_2 used in Eqs. (2), (11), and (12) are those fitted to DFTB results, listed in Table III. Even though this expression was derived only for

TABLE III. Parameters $k_\circ$, k_1, and k_2 used in Eqs. (2), (11), and (12) to estimate the different contributions to the deformation energy of a twisted nanotube rope as a function of the rope twist strain $\epsilon_\circ$ only. Values of k_1 and k_2 used in Fig. 3(d) are fitted to numerical DFTB results. Values of these quantities based on analytical expressions in the Appendix are listed for the sake of comparison.

Number of strands N_s	Chirality (n,m)	$k_\circ$ (eV) (DFTB fit)	k_1 (eV) (DFTB fit)	k_1 (eV) [Eq. (A11)]	k_2 (eV) (DFTB fit)	k_2 (eV) [Eq. (A12)]
2	(10,10)	3.08	2.61	2.60	−228.66	−18.53
6	(10,10)	3.09	19.86	23.95	−2723.69	−1176.86
7	(6,6)	3.16	18.11	30.77	−698.61	−1185.19
7	(18,0)	3.11	13.08	20.04	−1279.90	−479.33

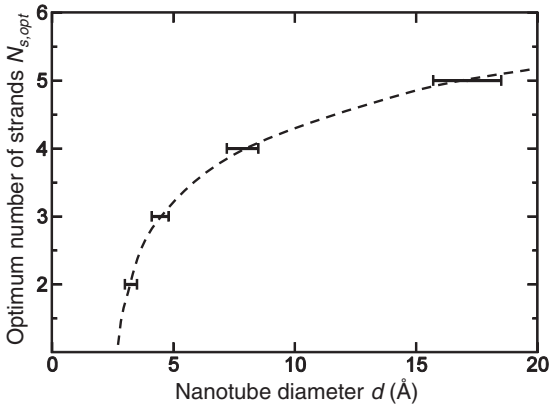

FIG. 5. Optimum number of nanotube strands $N_{s,\mathrm{opt}}$ that maximizes energy storage in ropes of carbon nanotubes with diameter d. The dashed line is a guide to the eye.

low twisting rates, we find these results to be in reasonable agreement with those of Fig. 4 in the entire elastic regime.

G. Optimum energy storage in a nanotube rope

As discussed above, the energy ΔE stored in a twisted nanotube rope is represented by Eq. (10). The individual energy contributions related to twisting, stretching, bending, and compression strains depend on the diameter of the constituent nanotubes. This energy is approximated by Eqs. (2), (11), and (12), which express $\Delta E/N$ only in terms of the twist strain $\epsilon_\circ$ of the entire rope. The dependence of $\Delta E/N$ on the diameter or related chirality of the constituent nanotubes becomes very obvious when comparing the values of k_1 and k_2 in Table III.

Obviously, the energy per atom stored in a twisted rope with N_s strands depends on the diameter of the constituent nanotubes. In turn, there is an optimum number of strands in a rope capable of storing the largest energy amount $\Delta E/N$ if the rope contains only nanotubes of a given diameter. The optimum number of nanotube strands $N_{s,\mathrm{opt}}$ may be estimated based on Eq. (A5) that is derived in the Appendix. The key consideration in these estimates is that the elastic limit is reached in different ways, which depend on the number of nanotube strands and the nanotube diameter. Even though the continuum elasticity extrapolation neglects anharmonic terms that cause softening, this limitation should not affect the main trend. Our results, presented in Fig. 5, indicate that energy storage density is maximized in relatively narrow nanotube ropes and that the optimum number of strands increases with nanotube diameter d. Even though the typical diameter range $10\,\text{Å} \lesssim d \lesssim 15\,\text{Å}$ of most abundant single-wall carbon nanotubes is relatively narrow, multiwall nanotubes have typically much larger diameters. Our calculations suggest that ropes with a large number of multiwall carbon nanotube strands should be very promising candidates for reversible energy storage.

IV. SUMMARY AND CONCLUSIONS

In conclusion, we used *ab initio* and parametrized density functional calculations to calculate the mechanical energy that can be stored reversibly in a twisted carbon nanotube rope. This energy storage mechanism, which bears resemblance with a twisted rubber band used to store energy in popular toys, yields unprecedented energy storage densities due the unusual toughness of carbon nanotubes. To realize the potential of a twisted nanotube rope as energy storage medium, nontrivial obstacles have to be overcome to retrieve this energy efficiently. For one, since the stored energy is quadratic in terms of displacement, controlled energy release requires careful consideration. In principle, this problem is identical to a spring in a mechanical watch, where constant energy delivery over time is regulated by an escapement mechanism. Encouraging first steps towards a practical realization of the storage mechanism are the observation of a torsional nanotube actuator[7] and the engineering design of a mechanism that converts energy stored in torsion to electrical energy.[9]

We find that a twisted nanotube rope may reversibly store energy by twisting, stretching, bending, and compressing constituent nanotubes. Our atomistic calculations allow us to determine the elastic deformation range and the associated energy storage density of twisted carbon nanotubes and nanotube ropes. Our results also reveal structural deformations beyond the elastic limit, where irreversibility is associated with breaking and forming new covalent bonds. An important insight provided by our study is that within the elastic regime, the interior of a twisted rope encounters hydrostatic pressures of up to tens of GPa. Since many substances can be intercalated in carbon nanotube ropes and thus be subjected to these high pressures, a twisted nanotube rope offers an attractive low-cost alternative to a diamond-anvil cell for high-pressure studies. Our atomistic calculations are complemented by a linear elasticity theory description of the combined energy storage mechanism that is not limited to single-wall carbon nanotube ropes. We find this description to adequately represent the atomistic results, to provide insight into the energy partitioning in a particular system, and to estimate the optimum rope diameter to optimize energy storage. Our analytical estimate indicates that the reversible mechanical energy storage capacity of twisted carbon nanotube ropes surpasses that of advanced Li-ion batteries by up to a factor of 10 in the optimum case. Secondary effects not included in this analytical estimate, including flattening of twisted nanotubes at the rope surface, may reduce this factor by about one half. Finally, in macroscopic realizations of this energy storage mechanism, additional problems may arise due to inadequate macroscopic contacts to nanoropes. It is beyond the scope of this study to judge whether a practical experimental realization of our nanomechanical energy storage mechanism will provide a viable alternative to the state of the art. We feel that our results, which, under optimum conditions, indicate a fourfold to tenfold increase in energy density over Li-ion batteries, are promising enough to justify experimental verification.

ACKNOWLEDGMENTS

We acknowledge valuable contributions to the computational approach by D.-B. Zhang and T. Dumitrica. This work was funded by the National Science Foundation Cooperative Agreement No. EEC-0832785, titled "NSEC: Center for High-rate Nanomanufacturing." G.S. was partly supported by

the European Centre for Emerging Materials and Processes Dresden (ECEMP, Project No. 10 13857/2379). The third author's visit to MSU was partially funded by the DAAD. Computational resources for this project were provided by the ZIH Dresden and the Michigan State University High-Performance Computer Center. We thank T. Moore for assistance with the visualization of structures.

APPENDIX

The equilibrium structure of a twisted nanotube rope may be characterized by the optimum twisting, stretching, bending, and compression strains of individual nanotubes and nanotube pairs. These deformations may be determined by optimizing the total energy expression in Eq. (10). This optimization may be performed analytically in view of the fact that the strains $\epsilon_\circ$, $\epsilon_{\parallel,i}$, $\epsilon_{\angle,i}$, and $\epsilon_{\perp,ij}$ are interrelated in a given twisted rope. Analytic expressions presented below allow us to analyze the relative significance of particular deformation modes and suggest ways to optimize energy storage.

In a twisted rope, the twist strain $\epsilon_\circ$ of each individual strain equals that of the entire rope. The axial strain $\epsilon_{\parallel,i}$ of the coiled strand i of the rope, represented schematically in the bottom panel of Fig. 3(a), is given by[4,32]

$$\epsilon_{\parallel,i} = \sqrt{1 + (\epsilon_\circ \rho_i / d_{(n,m)})^2} - 1, \tag{A1}$$

where ρ_i is the coil radius and $d_{(n,m)}$ the nanotube diameter. Similarly, the bending strain can be expressed as

$$\epsilon_{\angle,i} = \epsilon_\circ \frac{\epsilon_\circ \rho_i / d_{(n,m)}}{(\epsilon_\circ \rho_i / d_{(n,m)})^2 + 1}. \tag{A2}$$

When optimizing the rope geometry, we need to consider that the nanotube diameter is related to the intertube separation d_{ij}, which determines the coil radius ρ_i and also depends on the compression strain $\epsilon_{\perp,ij}$. This reduces significantly the number of independent variables for structure optimization. Optimization is easiest for ropes with symmetric cross sections. Ropes containing $N_s = 2,3,4$ nanotube strands do not have a central nanotube, in contrast to ropes with $N_s = 7,13,19$ nanotube strands that do have a nanotube in the center.

The maximum energy storage capacity for the individual deformation modes is listed in Table I. The theoretical maximum energy storage capacity $J = 12.35$ MJ/kg of a twisted rope then corresponds to the sum of storage capacities of all individual modes. This value could only be reached if all deformation modes were to reach the elastic limit simultaneously, which is practically never the case. In general, among the different deformation strains $\epsilon_\circ$, $\epsilon_{\parallel,i}$, $\epsilon_{\angle,i}$, and $\epsilon_{\perp,ij}$, the maximum reversible energy storage density in a twisted rope is determined by the deformation mode, which reaches the elastic limit first. The other deformation modes provide only a fraction of their maximum energy storage capacity.

To estimate the energy storage amount in a rope twisted to its elastic limit, we first introduce the new variable $x = \epsilon_\circ \rho_i / d_{(n,m)} = \rho_i \varphi / l_0$ that describes the deformation of nanotube strand i subject to the twist rate φ / l_0 in a coil of radius ρ_i. Then, Eq. (A1) reduces to

$$\epsilon_{\parallel,i} = \sqrt{1 + x^2} - 1 \tag{A3}$$

and Eq. (A2) to

$$\epsilon_{\angle} = \epsilon_\circ \frac{x}{x^2 + 1}. \tag{A4}$$

If there were no limit on x, then the maximum bending strain could be estimated using the expression in Eq. (A4). $\epsilon_{\angle}$ reaches its maximum at $x = 1$, yielding $\epsilon_{\angle,\max} = \epsilon_\circ / 2$ for the maximum bending strain. In reality, the allowed value range of x is limited by the elastic limit of the axial strain $\epsilon_{\parallel,\max} = 0.12$ according to Table I, which translates to $x \leqslant 0.50$ according to Eq. (A3) and thus to $\epsilon_{\angle} \leqslant 0.40\epsilon_\circ$. At the elastic limit of twisting $\epsilon_{\circ,\max} = 0.52$ according to Table I, we find $\epsilon_{\angle,\max} = 0.21$ for the maximum bending strain and the optimum coil radius $\rho_i / d_{(n,m)} = x / \epsilon_\circ = 0.97$.

We thus conclude that for specific twisted ropes, we may be able to simultaneously reach the elastic limits $\epsilon_{\circ,\max} = 0.52$, $\epsilon_{\parallel,\max} = 0.12$, and $\epsilon_{\angle,\max} = 0.21$. Neglecting compression, the sum of twisting, stretching, and bending deformation energies amounts to $J = 11.96$ MJ/kg if the ideal condition $x = \epsilon_\circ \rho_i / d_{(n,m)} = 0.97$ may be reached by all nanotube strands in a rope.

This condition may be achieved in a simple rope with N_s nanotube strands and no central nanotube. All nanotubes form corners of a polygon with N_s corners in cross section and share the same coiling radius ρ. Ignoring the difference between 0.97 and unity for the optimum value of $x / \epsilon_\circ = \rho / d_{(n,m)}$, we may approximate $d_{(n,m)} \approx \rho$. Considering the simple geometry of the polygonal cross section of the rope, where the nanotubes are separated by the interwall distance $d_{iw} \approx 3.0$–3.5 Å, we find

$$d_{(n,m)} = \frac{d_{iw}}{2 \sin(\pi / N_s) - 1}. \tag{A5}$$

Using Eq. (A5), we are able to estimate the optimum nanotube diameter that maximizes energy storage in a rope of N_s nanotubes. With the optimum nanotube diameters as a function of N_s at hand, we are able to present the optimum number of strands $N_{s,\mathrm{opt}}$ as a function of given nanotube diameter in Fig. 5. We need to point out the limits of the model ropes discussed here, since Eq. (A5) provides unphysical results for $N_s \geqslant 6$.

The value $J = 11.96$ MJ/kg achieved in the simplified rope due to twisting, stretching, and bending only is a significant fraction of the $J = 12.35$ MJ/kg, given by the sum of all decoupled deformations at their elastic limit according to Table I. In reality, the maximum storage values shown in Fig. 4 are lower since the optimum value $x = 0.97$ can not be reached by all nanotubes in a rope simultaneously.

Comparison of maximum achievable gravimetric energy storage densities J in Table I reveals that twisting is most important, followed by stretching, bending, and compression. The high-energy cost of twisting is mostly due to stretching and compression of C-C bonds, and only to a lesser degree to changes in bond angles, often called bond bending. Our structure optimization studies of isolated nanotubes indicate that stretching and bending primarily cause bond bending, which is a softer deformation mechanism. Neglecting the role of bond stretching in these deformations, we can relate the bending force constants to the stretching force constant by $k_{\angle} = k_{\parallel} / 12$. Using the value $k_{\parallel} = 32.5$ eV, given in Table I,

this estimate yields $k_\angle = 2.71$ eV, which is close to the value $k_\angle = 3.94$ eV that is listed in Table I. We also find the elastic limit of bending to be related to that of stretching by $\epsilon_{\angle,\max} = 2\epsilon_{\parallel,\max}$. Using the value $\epsilon_{\parallel,\max} = 0.12$ from Table I, we estimate $\epsilon_{\angle,\max} = 0.24$, in good agreement with the value 0.21 listed in Table I.

According to Table I, depending on the deformation path, the maximum energy density in a hydrostatically compressed nanotube array ranges from $J = 1.29$–4.62 MJ/kg, thus competing in significance with twisting and stretching. These values represent a rope with an infinite number of strands and no surface. Lower values occur in ropes with a finite number of strands since the compression energy scales with the number of pairs of adjacent nanotubes, which is reduced from 6 in the interior to as few as 3 at the rope periphery. In the extreme case of a 2-rope, the maximum values of J listed in Table I are reduced by a factor of 3.

Next we derive a simplified expression for the energy storage per atom $\Delta E/N$ as a useful counterpart of Eq. (10), which uses the deformations $\epsilon_\circ$, $\epsilon_{\parallel,i}$, $\epsilon_{\angle,i}$, and $\epsilon_{\perp,ij}$ as formally independent quantities. Our objective is to derive an energy expression that depends only on the twist strain $\epsilon_\circ$ that is externally applied to the entire rope. Using this expression, we intend to study the relative importance of the individual strains as a function of $\epsilon_\circ$.

In the following derivation, we will limit ourselves to ropes with a peripheral layer containing $N_{s,p}$ nanotube strands at a constant distance $\rho = \rho_p > 0$ from the center. Among these, we will consider ropes with a nanotube at the center, characterized by $\rho_c = 0$, or no central nanotube. Examples are ropes with two strands, described by $N_s = N_{s,p} = 2$, and with seven strands, described by $N_s = 7$ and $N_{s,p} = 6$. The nanotubes at the rope periphery form a regular polygon in cross section. Rather than specifying all intertube separations in terms of the equilibrium value $d_0 = d_{(n,m)} + d_{iw}$, we introduce the parameter λ, defined by $\lambda = \rho/[d_0(1-\epsilon_\perp)]$, which completely characterizes the geometry of a radially compressed rope. For nanotubes at equilibrium distance $d_0(1-\epsilon_\perp)$ along the rope periphery, we find $\lambda = [2\sin(\pi/N_{s,p})]^{-1}$. For small values of the rope twist strain $\epsilon_\circ$, Eqs. (A1) and (A2) may be rewritten as

$$\epsilon_\parallel \approx \frac{1}{2}\left(\frac{\lambda d_0}{d_{(n,m)}}\right)^2 (1-\epsilon_\perp)^2\epsilon_\circ^2 \qquad \text{and}$$
$$\epsilon_\angle \approx \frac{\lambda d_0}{d_{(n,m)}}(1-\epsilon_\perp)\epsilon_\circ^2. \tag{A6}$$

These relations simplify Eq. (10) to

$$\frac{\Delta E}{N} \approx \left[\frac{k_\parallel}{4}\left(\frac{\lambda d_0}{d_{(n,m)}}\right)^4 (1-\epsilon_\perp)^4 + k_\angle\left(\frac{\lambda d_0}{d_{(n,m)}}\right)^2 (1-\epsilon_\perp)^2\right] \times \frac{N_{s,p}}{N_s}\epsilon_\circ^4 + k_\circ\epsilon_\circ^2 + k_\perp\frac{N_\perp}{N_s}\epsilon_\perp^2, \tag{A7}$$

where $N_\perp$ is the total number of pairs of adjacent nanotubes in the rope. Examples are a 2-rope with $N_\perp = 1$ and a 7-rope with a central nanotube and $N_\perp = 12$.

At a given twist strain $\epsilon_\circ$, the optimum value of $\epsilon_\perp$ that minimizes the energy can be obtained from $\partial(\Delta E/N)/\partial\epsilon_\perp = 0$. This is equivalent to

$$k_\parallel\left(\frac{\lambda d_0}{d_{(n,m)}}\right)^4 (1-\epsilon_\perp)^3\epsilon_\circ^4 + 2k_\angle\left(\frac{\lambda d_0}{d_{(n,m)}}\right)^2 (1-\epsilon_\perp)\epsilon_\circ^4 - 2k_\perp\frac{N_\perp}{N_{s,p}}\epsilon_\perp = 0. \tag{A8}$$

Equation (A8) suggests that $\epsilon_\perp$ is a function of $\epsilon_\circ^4$. For small values, we obtain

$$\epsilon_\perp = \frac{1}{2k_\perp}\frac{N_{s,p}}{N_\perp}\left[k_\parallel\left(\frac{\lambda d_0}{d_{(n,m)}}\right)^2 + 2k_\angle\right] \times \left(\frac{\lambda d_0}{d_{(n,m)}}\right)^2\epsilon_\circ^4 + O(\epsilon_\circ^8). \tag{A9}$$

The approximation is valid for $\epsilon_\circ \lesssim 0.1$, before the terms of the order $O(\epsilon_\circ^8)$ become important.

With the above expressions we are now able to roughly estimate the energy dependence of the individual deformation mechanisms on the twist strain of the rope only. The energy contribution of twisting has an $\epsilon_\circ^2$ dependence. The energy contributions of stretching and bending have an $\epsilon_\circ^4$ dependence for $\epsilon_\circ \lesssim 0.1$. Correcting terms for these modes share the same $\epsilon_\circ^8$ dependence with compression. This analysis explains why twisting energy dominates at low values of $\epsilon_\circ$ and loses its leading role at higher twist rates.

The simplified energy storage expressions for the individual deformation modes may now be combined to

$$\Delta E/N \approx k_\circ\epsilon_\circ^2 + k_1\epsilon_\circ^4 + k_2\epsilon_\circ^8 + O(\epsilon_\circ^{12}), \tag{A10}$$

where

$$k_1 = \frac{N_{s,p}}{4N_s}\left[k_\parallel\left(\frac{\lambda d_0}{d_{(n,m)}}\right)^2 + 4k_\angle\right]\left(\frac{\lambda d_0}{d_{(n,m)}}\right)^2 \tag{A11}$$

and

$$k_2 = -\frac{1}{4k_\perp}\frac{N_{s,p}^2}{N_\perp N_s}\left[k_\parallel\left(\frac{\lambda d_0}{d_{(n,m)}}\right)^2 + 2k_\angle\right]^2\left(\frac{\lambda d_0}{d_{(n,m)}}\right)^4. \tag{A12}$$

Equations (A10)–(A12) correspond to Eqs. (2), (11), and (12).

Close inspection of Fig. 3(d) reveals that the functional form in Eq. (A10) reproduces the numerical DFTB results adequately in the range $\epsilon_\circ \lesssim 0.2$. The values of $k_\circ$, k_1, and k_2 used in the fitted functions of Fig. 3(d) are listed in Table III.

We found it instructive to compare these fitted values to estimates based on Eqs. (A11) and (A12). These estimates, obtained using $d_0 = d_{(n,m)} + d_{iw}$ with $d_{iw} = 3$ Å, are listed in Table III alongside the DFTB fits. For most nanotube ropes, we find the fitted values of $k_\circ$ to agree closely with the value $k_\circ = 3.14$ eV listed in Table I. With the exception of the 2-rope, the fitted values of k_1 are somewhat smaller than the values estimated using Eq. (A11). This reflects the fact that the elastic response due to stretching, bending, and compression is, to some degree, affected by the degree of torsion especially in ropes with many strands. The value of k_2 gains importance in Eq. (A10) especially at higher twist rates. All values of k_2 that are listed in Table III are negative since the elastic

response to torsion is expected to soften at high twist rates. There are sizable differences between the values fitted to DFTB calculations and those estimated using Eq. (A12), which is not surprising in view of the fact that energy contributions in Eq. (A10), which have k_2 as prefactor, are much smaller than those with k_1 as prefactor at small values of $\epsilon_\circ$, where this equation is valid. An additional reason for the differences in the listed values of k_2 is that the compression pathways found in the atomistic DFTB calculations of the ropes may differ somewhat from those found in infinite nanotube lattices. In spite of these limitations, we find the simple expression in Eq. (A10) to be surprisingly accurate and capable of semiquantitatively estimating the total energy storage capacity of a twisted nanotube rope.

*tomanek@pa.msu.edu

[1] C. Liu, F. Li, L.-P. Ma, and H.-M. Cheng, Adv. Mater. **22**, E28 (2010).

[2] R. Hammerschlag and C. P. Schaber, in *Energy Conversion*, edited by D. Y. Goswami and F. Kreith (CRC Press, Boca Raton, FL, 2008), Part 15, pp. 15–9.

[3] In *Carbon Nanotubes: Advanced Topics in the Synthesis, Structure, Properties and Applications*, Topics in Applied Physics No. 111, edited by A. Jorio, M. Dresselhaus, and G. Dresselhaus (Springer, Berlin, 2008).

[4] D. Teich, Z. G. Fthenakis, G. Seifert, and D. Tománek, Phys. Rev. Lett. **109**, 255501 (2012).

[5] D. Li, W. F. Paxton, R. H. Baughman, T. J. Huang, J. F. Stoddart, and P. S. Weiss, MRS Bull. **34**, 671 (2009).

[6] J. Foroughi, G. Spinks, G. Wallace, J. Oh, M. Kozlov, S. Fand, T. Mirfakhrai, J. Madden, M. K. Shin, S. J. Kim, and R. Baughman, Science **334**, 494 (2011).

[7] M. D. Lima, N. Li, M. Jung de Andrade, S. Fang, J. Oh, G. M. Spinks, M. E. Kozlov, C. S. Haines, D. Suh, J. Foroughi, S. J. Kim, Y. Chen, T. Ware, M. K. Shin, L. D. Machado, A. F. Fonseca, J. D. W. Madden, W. E. Voit, D. S. Galvão, and R. H. Baughman, Science **338**, 928 (2012).

[8] F. A. Hill, T. F. Havel, and C. Livermore, J. Micromech. Microeng. **19**, 094015 (2009).

[9] F. A. Hill, T. F. Havel, and C. Livermore, Nanotechnology **20**, 255704 (2009).

[10] B. I. Yakobson, C. J. Brabec, and J. Bernholc, Phys. Rev. Lett. **76**, 2511 (1996).

[11] B. I. Yakobson, Appl. Phys. Lett. **72**, 918 (1998).

[12] B.-W. Jeong, J.-K. Lim, and S. B. Sinnott, Appl. Phys. Lett. **90**, 023102 (2007).

[13] B.-W. Jeong, J.-K. Lim, and S. B. Sinnott, J. Appl. Phys. **101**, 084309 (2007).

[14] D. Qian, W. K. Liu, and R. S. Ruoff, Comput. Sci. Technol. **63**, 1561 (2003).

[15] J. Alford, B. Landis, and J. Mintmire, Int. J. Quantum Chem. **105**, 767 (2005).

[16] J. M. Soler, E. Artacho, J. D. Gale, A. García, J. Junquera, P. Ordejón, and D. Sánchez-Portal, J. Phys.: Condens. Matter **14**, 2745 (2002).

[17] D. M. Ceperley and B. J. Alder, Phys. Rev. Lett. **45**, 566 (1980).

[18] J. P. Perdew and A. Zunger, Phys. Rev. B **23**, 5048 (1981).

[19] N. Troullier and J. L. Martins, Phys. Rev. B **43**, 1993 (1991).

[20] L. Kleinman and D. M. Bylander, Phys. Rev. Lett. **48**, 1425 (1982).

[21] E. Artacho, D. Sánchez-Portal, P. Ordejón, A. García, and J. M. Soler, Phys. Status Solidi B **215**, 809 (1999).

[22] M. R. Hestenes and E. Stiefel, J. Res. Natl. Bur. Stand. **49**, 409 (1952).

[23] D. Porezag, T. Frauenheim, T. Köhler, G. Seifert, and R. Kaschner, Phys. Rev. B **51**, 12947 (1995).

[24] D.-B. Zhang, M. Hua, and T. Dumitrică, J. Chem. Phys. **128**, 084104 (2008).

[25] D.-B. Zhang and T. Dumitrica, Appl. Phys. Lett. **93**, 031919 (2008).

[26] D.-B. Zhang, R. D. James, and T. Dumitrica, Phys. Rev. B **80**, 115418 (2009).

[27] L. Zhechkov, T. Heine, S. Patchkovskii, G. Seifert, and H. A. Duarte, J. Chem. Theory Comput. **1**, 841 (2005).

[28] E. Ertekin and D. C. Chrzan, Phys. Rev. B **72**, 045425 (2005).

[29] See Supplemental Material at http://link.aps.org/supplemental/10.1103/PhysRevB.88.245402 for animations of structural changes induced by stretching, twisting, and compression of individual nanotubes and nanotube ropes.

[30] M.-F. Yu, O. Lourie, M. J. Dyer, K. Moloni, T. F. Kelly, and R. S. Ruoff, Science **287**, 637 (2000).

[31] Z. Zhu and D. Tománek, Phys. Rev. Lett. **109**, 135501 (2012).

[32] D. Teich, G. Seifert, S. Iijima, and D. Tománek, Phys. Rev. Lett. **108**, 235501 (2012).